Inorganic Chemistry

Article

pubs.acs.org/IC

Perovskite Metal Formate Framework of $[NH_2\text{-}CH^+\text{-}NH_2]Mn(HCOO)_3$]: Phase Transition, Magnetic, Dielectric, and Phonon Properties

Mirosław Mączka,*[,†] Aneta Ciupa,[†] Anna Gągor,[†] Adam Sieradzki,[‡] Adam Pikul,[†] Bogusław Macalik,[†] and Marek Drozd[†]

[†]Institute of Low Temperature and Structure Research, Polish Academy of Sciences, Box 1410, 50-950 Wrocław 2, Poland

[‡]Institute of Physics, Wrocław University of Technology, Wybrzeże Wyspiańskiego 27, 50-370 Wrocław, Poland

Supporting Information

ABSTRACT: We report the synthesis, crystal structure, and thermal, dielectric, phonon, and magnetic properties of $[NH_2\text{-}CH^+\text{-}NH_2][Mn(HCOO)_3]$ (FMDMn). The anionic framework of $[(Mn(HCOO)_3^-]$ is counterbalanced by formamidinium (FMD^+) cations located in the cavities of the framework. These cations form extensive N−H···O hydrogen bonding with the framework. The divalent manganese ions have octahedral geometry and are bridged by the formate in an *anti*−*anti* mode of coordination. We have found that FMDMn undergoes a structural phase transition around 335 K. According to the X-ray diffraction, the compound shows $R\bar{3}c$ symmetry at 355 K and $C2/c$ symmetry at 295 and 110 K. The FMD^+ cations are dynamically disordered in the high-temperature phase, and the disorder leads to very large bandwidths of Raman and IR bands corresponding to vibrations of the NH_2 groups. Temperature-dependent studies show that the phase transition in FMDMn is associated with ordering of the FMD^+ cations. Detailed analysis shows, however, that these cations still exhibit some reorientational motions down to about 200 K. The ordering of the FMD^+ cations is associated with significant distortion of the anionic framework. On the basis of the magnetic data, FMDMn is a weak ferromagnet with the critical temperature T_c = 8.0 K.

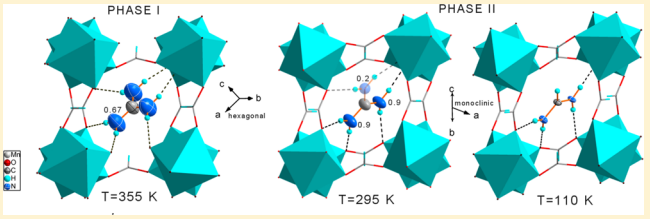

INTRODUCTION

Metal−organic frameworks (MOFs) have emerged as a promising class of compounds for various applications due to the huge number of organic ligand and metal ion combinations that offer the possibility of a systematic tuning of their physicochemical properties. Thus, MOFs have been found to be prospective materials for gas storage and sensor applications.[1] Many of them are also attractive ferroelectric materials.[2] In recent years, a new emerging route for the preparation of multiferroic materials with tailored magnetic and ferroelectric properties was proposed, i.e., synthesis of metal−organic frameworks containing magnetic ions.[3] Especially promising are metal−organic frameworks with formate ligands and divalent cations. Multiferroic properties were found in a few compounds of formula $[Cat][M(HCOO)_3]$ with M = Mn, Ni, Co, Fe, Cu and cat = ammonium and dimethylammonium (DMA).[4−6] Coexistence of electric and magnetic order was also predicted theoretically for some formates containing cat = guanidinium (GUA), and ethylammonium cation, but it has not yet been confirmed experimentally.[7−10]

The ability of the DMA^+ to act as a template in the growth of metal formates is widely described in the literature.[4−6,11] On the contrary, the FMD^+ cation is less investigated. There are some reports on the synthesis of $[FMD][M(HCOO)_4]$ formates with M = Eu, Gd, Tb, Dy, Er, Yb, which showed remarkable emission intensity.[12] In the case of formates containing divalent cations, only two compounds are known, i.e., $[FMD][Zn(HCOO)_3]$ and $[FMD][Mg(HCOO)_3]$.[13] These compounds crystallize in the orthorhombic *Pnna* space group, with the FMD^+ cations located in the lattice channels.[13] In contrast to the formates containing DMA^+ cations, the FMD^+ cations are ordered in the known formates, and there are no reports on any phase transformations. However, if the cavities occupied by FMD^+ cations are large enough, these ions may also exhibit disorder and sequence of phase transitions associated with their ordering. Such behavior was observed, for instance, for the $FMDPbI_3$ compound.[14]

Herein, we report the synthesis, structure, and thermal, dielectric, vibrational, and magnetic properties of the novel FMDMn compound. We will show that the structure of this compound is different from the structure of known Zn and Mg analogues. We will also show that FMDMn undergoes a structural phase transition, and we will discuss the mechanism of this phase transition.

EXPERIMENTAL SECTION

Synthesis. $MnCl_2$ (99%, Aldrich), formamide (99.5%, Aldrich), and cyclobutane-1,1′-dicarboxylic acid (99%, Aldrich) were commercially available and used without further purification. Elemental analysis (C, H, N) was performed on a Elementar Vario EL CHNS analyzer. Crystals were prepared under solvothermal conditions at 130 °C. In this method, formamidinium and formate ions are formed through hydrolysis of formamide under high temperature and

Received: February 28, 2014
Published: April 30, 2014

   dx.doi.org/10.1021/ic500479e | Inorg. Chem. 2014, 53, 5260−5268

pressure. This synthesis method is an adaptation of the previously reported one for the preparation of [FMD][Mg(HCOO)$_3$].[13] In a typical experiment, a mixture of $MnCl_2$ (8.4 mmol), formamide (50 mL), and cyclobutane-1,1′-dicarboxylic acid (4.2 mmol) was heated in a Teflon-lined microwave autoclave for 24 h. After slow overnight cooling, light pink crystals were collected, washed with ethanol (3 × 5 mL), and dried at room temperature. The yield was about 85% based on the starting manganese salt. A good match of its powder XRD pattern with the calculated one based on the single-crystal structure (see Figure S1 in the Supporting Information) confirmed the phase purity of the bulk sample. Anal. Calcd: C, 20.43; H, 3.41; N, 11.92. Found: C, 20.21; H, 3.38; N, 11.79.

Heat Capacity. Heat capacity was measured using a Mettler Toledo DSC-1 calorimeter with a high resolution of 0.4 μW. Sample weight was chosen to be 12.61 mg. The sample was slightly crushed to ensure good thermal contact. Nitrogen was used as a purging gas. The temperature change rate was chosen to be 5 K/min, and the DSC thermograms were taken for both cooling and heating cycles. The excess heat capacity associated with the phase transition was calculated by subtraction from the data the baseline representing variation in the absence of the phase transitions.

Dielectric Properties. The complex dielectric permittivity was measured using a broadband impedance Alpha analyzer with an Active Sample Cell (Novocontrol). The measurements were taken every 1 deg over the temperature range from 87 to 390 K on a pellet made of well-dried sample. The pellet had a diameter of 6 mm and thickness of 0.5 mm, and it was located between gold electrodes with a diameter of 6 mm. The sample was located in the sample chamber filled by dry nitrogen. The temperature was changed by flow of heated, vaporized liquid nitrogen and controlled by a self-made heating system. The temperature stabilization was ±0.2 K.

The complex dielectric function is given by $\varepsilon''(\omega) = \varepsilon' - i\varepsilon'' = -i/(\omega Z^*(\omega)C_0)$, where Z^* is the measured complex impedance, C_0 is the geometrical capacitance of the sample, and $\omega = 2\pi f$ is the angular frequency. All measurements including the calibration routine, temperature stabilization, and data acquisition were automatically controlled.

Magnetic Properties. Magnetic properties of a large number of freely oriented single crystals of FMDMn (about 30 mg in total) were measured on a commercial Quantum Design superconducting quantum interference device (SQUID) magnetometer in the temperature range 2−25 K and in external magnetic fields up to 1.5 kOe. The background coming from the weakly diamagnetic sample holder (not shown here) was found to be negligible; thus its subtraction was omitted. Also no demagnetization corrections were made to the data reported here.

Crystal Structure Determination. Single-crystal diffraction data were collected at 355, 295, and 110 K on a KM4-CCD diffractometer operating in κ geometry and equipped with a two-dimensional CCD detector. Mo Kα radiation (0.71073 Å) was used. Data were collected in ω-scan mode with $\Delta\omega = 1.0°$ using the CrysAlis CCD program. CrysAlis RED software version 1.170.32 (Oxford Diffraction) was used for data processing.[15] The structures were solved by direct methods and refined using full-matrix least-squares methods with the SHELXL-97 program package.[16] Multiscan absorption collection was applied on all data. The geometrical parameter restraints (DFIX) were used to fix disordered FMD^+ cations to be chemically reasonable in $C2/c$ phase at room temperature. Hydrogen atoms were placed in calculated positions and refined as riding atoms at 295 and 355 K. At low temperature phase positions of hydrogen atoms from the FDM^+ counterion were refined. Thermal parameters of hydrogen atoms were set to be equal to 1.2 times the thermal parameters of the corresponding parent atoms. High temperature was maintained in a simple high-temperature attachment with a hot-air flow (Kuma Diffraction, covering the temperature range 300−770 K), while an open flow nitrogen cryosystem (Oxford Cryosystem, covering the temperature range 90−320 K) was used for experiments at low temperatures. The results of the data collection and refinement along with the crystal description are presented in Table S1.

The XRD pattern of FMDMn was also obtained on an X'Pert PRO X-ray diffraction system equipped with a PIXcel ultrafast line detector and Soller slits for Cu Kα_1 radiation (λ = 1.54056 Å).

Raman and IR Studies. Raman spectra in the 5−295 K (295−450 K) range were measured using a Bruker FT 100/S spectrometer with Nd:YAG laser excitation (1064 nm) and a helium-flow Oxford cryostat (Linkam cryostat cell THMS600). Additional low-frequency Raman spectra were measured using a Renishaw InVia Raman spectrometer equipped with a confocal DM 2500 Leica optical microscope, a thermoelectrically cooled CCD as a detector, and a diode laser operating at 830 nm. The sample for low-frequency measurements was put in a Linkam THMS600 cryostat cell. IR spectra in the range 3800−400 cm^{-1} (500−50 cm^{-1}) and at a temperature of 5−295 K were measured for the sample in a KBr pellet (Apiezon N suspension) with a Biorad 575C FT-IR spectrometer using a helium-flow Oxford cryostat. IR spectra in the range 3800−400 cm^{-1} (500−50 cm^{-1}) and at a temperature of 295−470 K were measured for the sample in a KBr (CsI) pellet using a homemade furnace. The resolution was 2 cm^{-1}.

RESULTS

Thermal Properties. The DSC measurements show a clear anomaly at 336.6 K upon heating and 334.3 K upon cooling (Figure S2). The change in the heat capacity and entropy related to the phase transition is presented in Figure 1. The

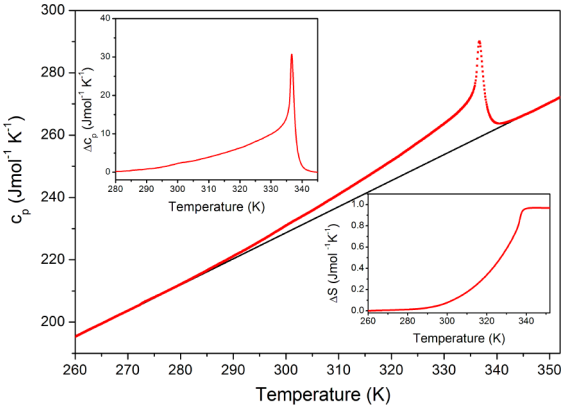

Figure 1. Heat capacity of FMDMn measured in a heating mode. The insets show the change in C_p and S related to the phase transition.

ΔC_p and ΔS become gradually larger with increasing temperature from about 280 K to about 334 K. With further increase in temperature, ΔS exhibits a weak but sharp increase, followed by no change above 336.8 K, whereas ΔC_p exhibits a sharp peak centered at 336.8 K. Such temperature dependence of ΔC_p and ΔS suggests that the phase transition has a slightly first-order character.

The associated change in enthalpy ΔH and entropy ΔS arising from the phase transition was estimated to be ∼0.360 kJ mol^{-1} and ∼0.97 J mol^{-1} K^{-1}, respectively. According to our X-ray diffraction studies, the FMD^+ cation shows trigonal disorder in the high-temperature (HT) phase (see discussion in the next paragraphs of the present paper). For an order−disorder transition, $\Delta S = R\ln(N)$, where N is the number of sites for the disordered system. Therefore, for a simple 3-fold order−disorder model ΔS should be 9.1 J mol^{-1} K^{-1}. Our data show that ΔS is an order of magnitude smaller than the expected value. This result indicates that the phase transition is more complex than expected on the basis of a simple 3-fold order−disorder model. It is worth noting that a less than expected entropy change at a phase transition is known in the multiferroic family. It was, for instance, observed for

dx.doi.org/10.1021/ic500479e | Inorg. Chem. 2014, 53, 5260−5268

$(NH_4)_3Cr(O_2)_4$ and $M_{3-x}(NH_4)_xCrO_8$ (M = Na, K, Rb, Cs) multiferroics.[17] It has been discussed that this behavior is observed since some residual entropy is always left over if the transition has some relaxor character.[17] As discussed below, our dielectric studies show the presence of a clear relaxation process in the here-studied FMDMn.

Dielectric Properties. Figure 2 shows the temperature dependences of the real (ε') and imaginary (ε'') part of the

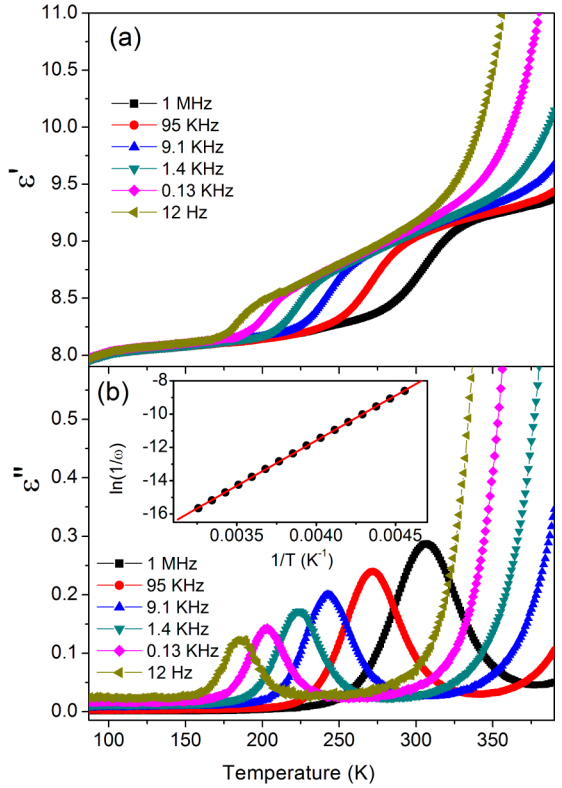

Figure 2. The real (a) and imaginary (b) part of the complex dielectric constant of FMDMn at different frequencies. Inset shows the Arrhenius plot for the dielectric relaxation.

complex dielectric function as a function of frequency. Figure 2 shows that ε' exhibits a step-like change, which shifts toward higher temperatures with increasing frequency. The imaginary part ε'' exhibits a broad peak just where the ε' increases most steeply (Figure 2). This type of temperature dependence is characteristic of the Debye-type dielectric relaxation, in which the reorientation of dipoles cannot respond to the applied ac electric field with high frequency exceeding a relaxation rate $1/\tau$. In such case ε' and ε'' are expressed by the following equations:

$$\varepsilon'(\omega) = \frac{\varepsilon_0 - \varepsilon_\infty}{1 + \omega^2\tau^2} + \varepsilon_\infty \quad (1)$$

$$\varepsilon''(\omega) = \frac{(\varepsilon_0 - \varepsilon_\infty)\omega\tau}{1 + \omega^2\tau^2} \quad (2)$$

where τ, ω, ε_0, and ε_∞ are the relaxation time, frequency, static dielectric constant, and high-frequency dielectric constant, respectively. Figure 2 shows that the maximum of ε'' shifts very strongly, that is, by about 120 K from low to high frequencies. The Cole–Cole diagram (Figure 3) exhibits almost symmetric semicircles, characteristic for the Debye-type dielectric relaxation with a single relaxation. It should be

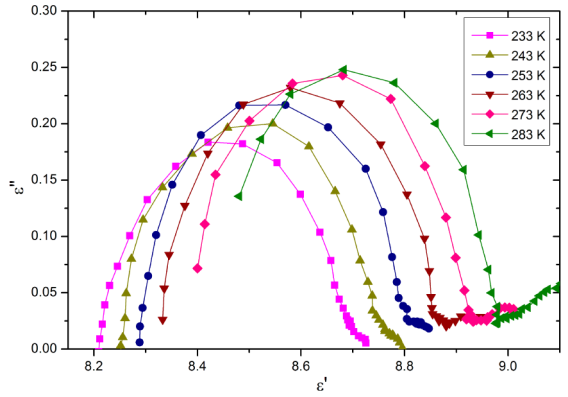

Figure 3. Cole–Cole diagram of FMDMn at a few temperatures.

noticed that this relaxation is even larger than that reported by us for $[(CH_3)_2NH_2][Ni(HCOO)_3]$ (78 K) and $[(CH_3)_2ND_2][Ni(HCOO)_3]$ (86 K).[11] The dielectric relaxation observed below T_c obeys the Arrhenius low for $\tau = \omega^{-1}$ as a function of T, with $\tau_0 = 3.8 \times 10^{-15}$ s and $E_a/k_B = 5.4 \times 10^3$ K ≈ 0.46 eV. In the HT phase, the FMD^+ cations are disordered, and a hopping motion of these cations between three orientations is responsible for the dielectric dispersion. The activation energy for reorientational motion of the FMD^+ cation in FMDMn is significantly larger (E_a = 0.46 eV) than that found in $[(CH_3)_2NH_2]Zn(HCOO)_3]$ (E_a = 0.24 eV).[18]

Magnetic Properties. Figure 4 displays temperature dependence of the magnetization, $M(T)$, of FMDMn measured

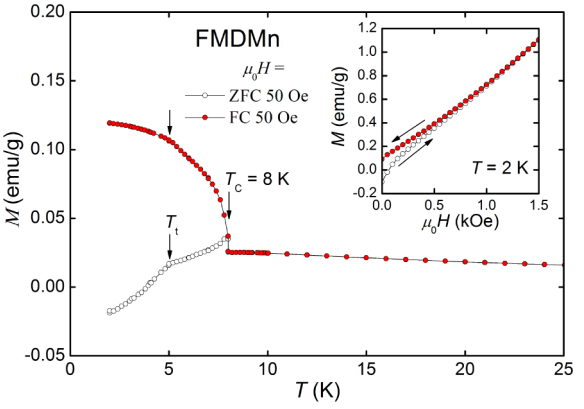

Figure 4. Temperature variation of the magnetization M of FMDMn measured in the zero-field-cooling (ZFC) and field-cooling (FC) regimes. Inset: Magnetization as a function of the external magnetic field μ_0H. Solid lines serve as a guide for the eye, and the arrows mark the ordering temperature T_m and the spin-reorientation temperature T^*.

in an external magnetic field of 50 Oe under zero-field-cooling (ZFC) and field-cooling (FC) conditions. As seen, in both cases the magnetization of the compound exhibits a distinct anomaly at T_m = 8.0(2) K, followed by another, less visible feature at about 5 K. The Brillouin-like shape of the M(T) curves in the FC regime manifests a ferromagnetic-like character of the phase transition at T_m. A small hysteresis in M measured as a function of the external magnetic field (see the inset to Figure 4) seems to corroborate the latter hypothesis; it is visible only at low fields, well below 1 kOe. The second anomaly in M(T) might arise from a spin-reorientation. It is worth noting that MOFs have a likelihood of glassy behavior, as

dx.doi.org/10.1021/ic500479e | Inorg. Chem. 2014, 53, 5260–5268

seen in the related $[(CH_3)_2NH_2][Zn(HCOO)_3]$,[19] and the second anomaly could also be related to the glass phase. However, assuming long-range order below T_m, the spin-glass behavior below T_t is not likely. Nevertheless, further investigations, especially an NMR study like that preformed by Besara et al. for $[(CH_3)_2NH_2][Zn(HCOO)_3]$,[19] are needed to obtain information if FMDMn also exhibits a glassy behavior at low temperatures.

A large difference between the FC and ZFC curves and especially the negative magnetization observed in the ZFC regime at the lowest temperatures are characteristic of weak ferromagnetism, which is often caused by a small canting of the underlying antiferromagnetic lattice. Such a small canting is in general strongly sensitive to the temperature, magnetic field, and the strength of the coupling between the magnetic ions. Small changes in these parameters may lead to complex magnetic behavior and even to reversal of the magnetization sign with decreasing temperature below a certain compensation temperature.[11,20] The canting may result from an antisymmetric exchange or single-ion anisotropy,[21] which are very likely in the compound studied. Moreover, neutron diffraction experiments are strongly needed to reveal the details of the magnetic structure of FMDMn.

Structural Studies. The crystallographic data obtained at different temperatures are summarized in Tables 1 and S2.

Table 1. Selected Distances (Å) in FMDMn

	355 K		295 K	110 K
6 × Mn1−O1	2.1871(9)	2 × Mn1−O2	2.1759(13)	2.1794(8)
		2 × Mn1−O1	2.1793(14)	2.1799(8)
		2 × Mn1−O3	2.1918(14)	2.1942(8)
O1−C1	1.231(2)	O1−C2	1.233(2)	1.246(2)
		O2−C2	1.234(2)	1.254(2)
		O3−C1	1.244(2)	1.254(1)
C2−N1	1.229(3)	N1−C3	1.273(3)	1.298(2)
		C3−N2	1.279 (1)	

FMDMn crystallizes in the monoclinic system in the centrosymmetric space group $C2/c$. At around 340 K the structure transforms to the rhombohedral system with $R\bar{3}c$ symmetry. In the parent phase the divalent manganese ions occupy the S_6 (D_{4d}) symmetry site and are octahedrally coordinated by the formate ligands. The Mn−O distances are equal to 2.1871(9) Å at 355 K (see Table 1). The octahedra are bridged together by the formate groups in an *anti*−*anti* mode configuration, forming a 3D pseudoperovskite substructure. The closest Mn−Mn distances via the bridging $HCOO^-$ are equal to 6.0772(1) Å at 355 K.

The FMD^+ counterions are located in large cavities within the $[Mn(COOH)_3^-]$ framework to which they are hydrogen bonded (with the donor to acceptor ($D\cdots A$) distance of 2.8776(18) Å and the donor to acceptor angle of 167°; see Table 2). The hydrogen bonds are, however, too weak to overcome the thermally activated motions, and the FMD^+ ions are dynamically disordered within three symmetrically equivalent positions around the 3-fold axis in the high-temperature phase; see Figure 5.

Below 340 K the crystal structure deformation leads to the lowering of the crystal symmetry. The mechanism of the phase transition is complex. The ordering of FMD^+ ions is conjugated to the lattice deformation. Figure 6 shows the thermal evolution of the lattice parameters that experience discontinuous changes

Table 2. Geometries of the N−H···O Hydrogen Bonds between the FMD^+ Cations and the Anionic Framework

D−H···A[a]	D−H (Å)	H···A (Å)	D···A (Å)	D−H···A (deg)
355 K				
N1−H1A···O1	0.86	2.03	2.8776 (18)	167.0
295 K				
N1−H1A···O2^{i}	0.87	2.01	2.862 (3)	165.4
N1−H1B···O3^{ii}	0.84	2.07	2.897 (3)	165.3
N2−H3A···O1	0.86	1.96	2.792 (2)	163.5
110 K				
N1−H1A···O2^{i}	0.84 (2)	2.03 (2)	2.8570 (15)	170.0 (17)
N1−H1B···O3^{ii}	0.842 (19)	2.06 (2)	2.8984 (15)	171.8 (16)

[a]Symmetry code(s): (i) $-x+1/2, y+1/2, -z+1/2$; (ii) $-x+1/2, -y+3/2, -z$.

at the transition temperature. The most affected are the b and c parameters (with $\Delta b/b$ and $\Delta c/c \approx 1\%$), which refer to the distances between two closest, nonbridged manganese ions. The changes disturb also the Mn−Mn distances via the bridging $HCOO^-$ ligands, which decrease to 6.0137(2) and 6.0435(2) Å at 110 K. It is interesting to notice that in the HT phase both parameters exhibit either weak temperature dependence or a usual decrease upon cooling, whereas in the low-temperature (LT) phase the parameter c increases upon cooling (see Figure 6). Negative thermal expansion has recently been reported also for $[NH_4][Mg(HCOO)_3]$ and $[NH_3(CH_2)_4NH_3][Mg(HCOO)_3]$ formates, and it has been argued that the librational motions of ammonium ions provide the underlying mechanisms for NTE in these compounds.[22] The ordered FMD^+ cations in the $C2/c$ space group accommodate C_2 symmetry. At room temperature 20% of the counterions are still disordered and the FMD^+ cations occupy three positions, one with probability 80% and two equivalent orientations with 10% probability; see Figure 5. Temperature lowering leads to further ordering of the FMD^+ cations, which at 110 K occupy only one position and form two hydrogen bonds to the oxygen atoms of the formate groups. Namely, N(1)−H1A···O2, with a $D\cdots A$ distance of 2.8570(15) Å and DHA angle of 170.0, and N1−H1B···O3, with a $D\cdots A$ distance of 2.8984(15) Å and DHA angle of 171.8° (see Table 2). The phase transition affects also the metal coordination sphere, which changes from distorted trigonal to distorted octahedron of the C_i point group with Mn−O distances ranging from 2.1794(8) to 2.1942(8) Å. The content of the asymmetric unit in both phases together with the atom-numbering scheme is shown in Figure S3, Supporting Information.

Vibrational Studies: Selection Rules and Assignment of Modes. The vibrational modes of the studied compound may be subdivided into internal vibrations of the FMD^+ and formate ions and the lattice vibrations. As already discussed in previous papers, the free $HCOO^-$ ion has C_{2v} symmetry, and its six fundamental internal vibrations can be classified as ν_1 (C−H stretching), ν_2 (symmetric C−O stretching), ν_4 (antisymmetric C−O stretching), ν_3 (symmetric O−C−O bending), ν_5 (C−H in-plane bending), and ν_6 (C−H out-of-plane bending) modes.[11,23] Since both the room-temperature phase (space group $R\bar{3}c$) and low-temperature phase (space group $C2/c$) comprise six $HCOO^-$ ions in the primitive cell, the number of internal modes of $HCOO^-$ ions is 36 in both phases, as presented in Table S3. The free FMD^+ cation also has C_{2v} symmetry, and the 18 internal modes are distributed among the

dx.doi.org/10.1021/ic500479e | Inorg. Chem. 2014, 53, 5260−5268

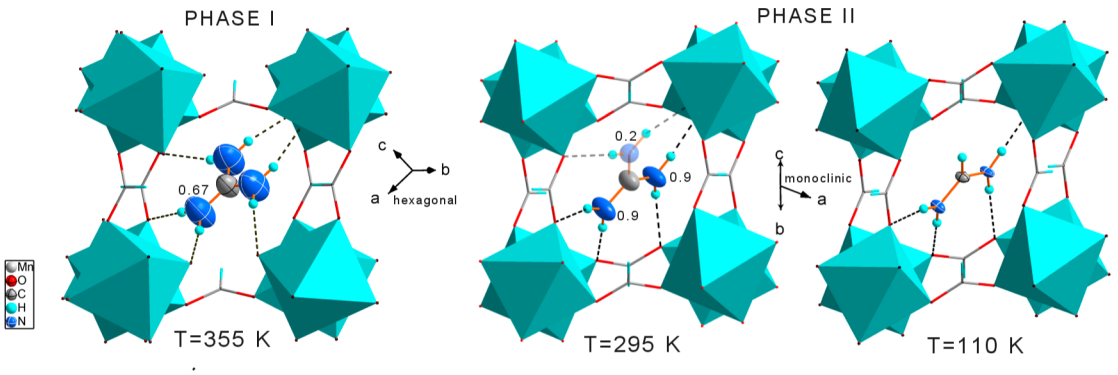

Figure 5. Ordering of the FMD^+ counterions with temperature lowering. Site occupation factors are drawn for the nitrogen atoms. Dashed lines represent hydrogen bonds.

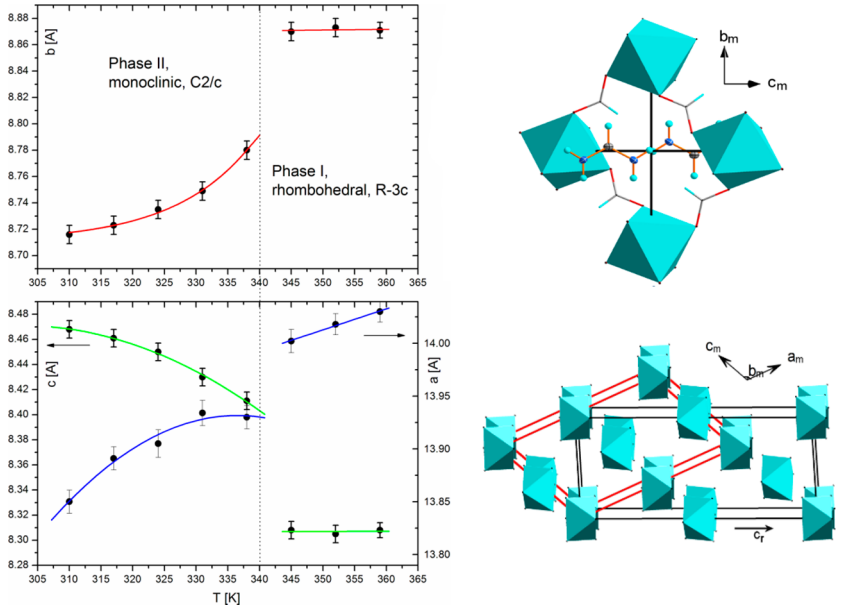

Figure 6. Thermal evolution of the monoclinic unit cell dimensions in FMDMn crystals during heating. The phase transition affects all lattice parameters, $b_{mono} = a_{hex}$. Monoclinic b and c parameters refer to the distances between nonbridged Mn centers. Solid lines are shown to guide the eye.

irreducible representation: $\Gamma = 7A_1 + 2A_2 + 6B_1 + 3B_2$. Similarly as shown previously for the DMA^+ cation, vibrations of the NH_2 group can be subdivided into symmetric stretching ($\nu_s(NH_2)$), antisymmetric stretching (($\nu_{as}(NH_2)$), scissoring ($\delta(NH_2)$), rocking ($\rho(NH_2)$), wagging ($\omega(NH_2)$), and torsion or twisting ($\tau(NH_2)$) modes.[11] However, the number of these vibrations is doubled when compared to DMA^+, due to the presence of two NH_2 groups in the FMD^+ cation. The remaining skeletal modes of FMD^+ cations are symmetric stretching ($\nu_s(CN)$), antisymmetric stretching ($\nu_{as}(CN)$), and bending ($\delta(CN)$) modes of the NCN group, as well as stretching ($\nu(CH)$), in-plane bending ($\delta(CH)$), and out-of-plane bending ($\gamma(CH)$) modes of the C−H group (see Table S3). Since the FMD^+ cation is disordered in the $R\bar{3}c$ phase, we present the distribution of the vibrational modes of FMD^+ among the irreducible representation only for the ordered $C2/c$ structure (see Table S3).

The Raman and IR spectra of FMDMn are presented in Figures 7−9 and S4−S6, Supporting Information. The observed IR and Raman frequencies (in cm^{-1}) are listed in Table S4, Supporting Information together with suggested assignments. The assignment of bands corresponding to

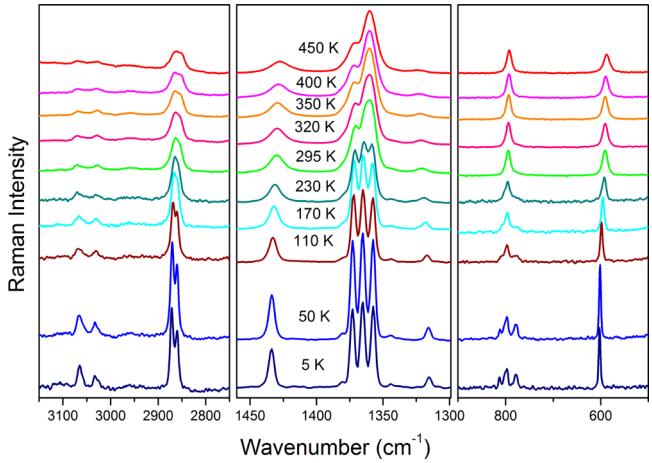

Figure 7. Enlarged parts of the Raman spectra showing details in the spectral ranges 2750−3150, 1300−1460, and 500−900 cm^{-1}.

vibrations of the $HCOO^-$ and Mn^{2+} ions could easily be done by comparison with the spectra of other related metal

dx.doi.org/10.1021/ic500479e | Inorg. Chem. 2014, 53, 5260−5268

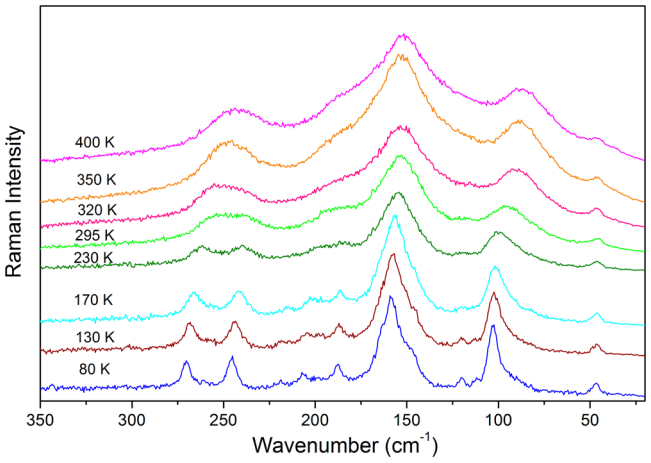

Figure 8. Raman spectra of FMDMn measured using a Renishaw InVia Raman spectrometer and eclipse filter at various temperatures corresponding to the spectral range 20−350 cm^{-1}. The spectra were normalized by the Bose−Einstein factor.

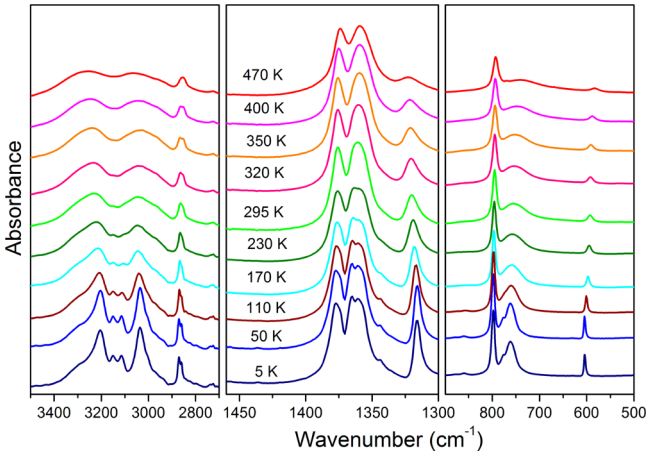

Figure 9. Details of the IR spectra results corresponding to the spectral ranges 2700−3500, 1300−1460, and 500−900 cm^{-1}.

formates with DMA^+ and NH_4^+ cations, discussed recently by us.[11,22] Vibrational properties of compounds containing the FMD^+ ion hasve not been extensively discussed in the literature. Nevertheless, we propose assignment of modes of the FMD^+ ion by comparison of present results with literature data reported for compounds containing other ammonium cations such as DMA^+ and GUA^+.[11,24]

Temperature-Dependent Raman and IR Studies. Raman and IR spectra exhibit pronounced changes upon cooling the sample below T_c. In particular, the majority of bands split into a few components and many new bands appear, especially in the lattice mode region below 400 cm^{-1}. According to the correlation diagram presented in Table S3, due to a decrease of the symmetry from $R\bar{3}c$ to $C2/c$ below T_c, splitting is expected for the E_u and E_g modes of the metal formate framework. Moreover, A_{2g} (A_{1u}) silent modes should become Raman-active (IR-active), giving rise to new bands below T_c. An especially large increase in the number of bands is expected in the lattice mode region. For instance, the number of Raman (IR) bands related to lattice modes of the $HCOO^-$ and Mn^{2+} ions should increase from 8 (11) for the $R\bar{3}c$ phase to 18 (21) for the $C2/c$ phase. Thus, the large increase in the number of lattice modes below T_c observed by us is consistent with the proposed symmetry change from $R\bar{3}c$ to $C2/c$.

In order to understand the structural changes occurring at the phase transition, we present the temperature dependence of a few selected vibrational frequencies of FMDMn (Figures 10,

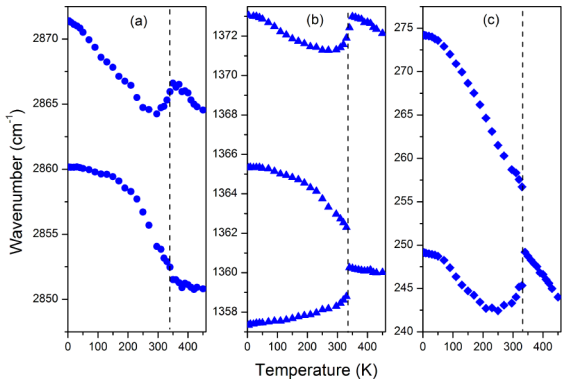

Figure 10. Temperature evolution of (a) $\nu_1(HCOO^-)$, (b) $\nu_2(HCOO^-)$ and $\nu_5(HCOO^-)$, and (c) $T'(HCOO^-)$ mode Raman frequencies. The vertical lines indicate the temperature at which FMDMn undergoes a phase transition.

S7, and S8). Figure 10b,c show that the 245 and 1360 cm^{-1} Raman modes exhibit significant splitting near T_c, and this splitting increases in a continuous way upon further cooling. Frequencies of the 2871 ($\nu_1(HCOO^-)$), 1373 ($\nu_5(HCOO^-)$), and 602 cm^{-1} ($\tau(NH_2)$) Raman modes (at 5 K) exhibit a continuous increase upon cooling the high-temperature phase from 450 K to around 340 K. Near 340 K, a clear decrease in frequency is observed for these modes (see Figures 10a,b and S7). The observed decrease is however not very sharp but extends down to about 295 K. Upon further cooling the sample, frequencies of these modes exhibit a further increase. The observed temperature dependence of the discussed modes provides important information on structural changes in FMDMn. First, weak discontinuity of the splitting and lack of discontinuous frequency shifts indicate that the phase transition has slightly first-order nature. Second, the large magnitude of the observed splitting at 5 K, 25 cm^{-1} for the $T'(HCOO^-)$ and 8 cm^{-1} for the $\nu_2(HCOO^-)$ modes, as well as downshifts of the discussed $\nu_1(HCOO^-)$ and $\nu_5(HCOO^-)$ modes at T_c by 1.7 and 2.4 cm^{-1}, respectively, points to a significant distortion of the metal formate framework below T_c. In particular, the splitting of the C−O symmetric stretching mode ν_2 indicates that the two C−O bonds in the $HCOO^-$ ion no longer have equal lengths in the low-temperature phase. Third, in contrast to the $HCOO^-$ modes, the 1741, 1428, 1091, and 761 cm^{-1} modes of the formamidine ion do not show any clear frequency shifts near T_c, although a clear change in the slope of frequency versus temperature can be noticed (see Figures S7 and S8). A very weak shift toward lower frequencies near T_c (about 0.2 cm^{-1}) is observed only for the Raman-active mode at 602 cm^{-1} (see Figure S7). This behavior indicates that the phase transition does not lead to any significant distortion of the formamidinium ion. This behavior is significantly different from that observed for the dimethylammonium analogue, for which very clear shifts toward higher frequencies were observed for DMA^+ modes at T_c, suggesting significant distortion of the these ions in the low-temperature phase.[11]

Let us now discuss the H-bond strength and its temperature dependence. Temperature-dependent IR spectra show that

dx.doi.org/10.1021/ic500479e | Inorg. Chem. 2014, 53, 5260−5268

some of the broad bands observed in the 3000−3300 cm^{-1} range, which correspond to the N−H stretching modes, soften with a decrease in temperature; that is, they shift from 3253 and 3060 cm^{-1} at 470 K to 3203 and 3035 cm^{-1} at 5 K (see Figure 9 and Table S4). The N−H stretching vibrations of isolated amine molecules are usually observed in the 3300−3500 cm^{-1} region.[24,25] Intermolecular interactions via H-bonds lead to a significant shift of the stretching modes toward lower frequencies as well as an increase of intensity and bandwidth of the corresponding bands.[25,25] Our spectra measured at 470 K show that the N−H stretching modes are observed at about 200−300 cm^{-1} lower frequency than expected for free amine molecules. Furthermore, they exhibit softening upon cooling. This result indicates that the N−H···O H-bonds in the studied compound are of medium strength, and the strength of H-bonds significantly increases upon cooling. Similar behavior was also reported for the dimethylammonium analogue.[11]

Decreasing of temperature leads also to significant changes in full width at half-maximum (fwhm) of many bands. Figure S9 shows that fwhm values of the T′($HCOO^-$), ν_2($HCOO^-$), and ν_5($HCOO^-$) Raman modes weakly decrease until T_c and then exhibit a fast decrease below T_c. The fwhm values decrease upon cooling to 5 K by about to 2−3 times for internal modes of the $HCOO^-$ units and even up to 8 times for the lattice modes. An even more pronounced decrease in fwhm values, by about 5 times, is also observed for the 761 and 604 cm^{-1} bands, corresponding to the ω(NH_2) and τ(NH_2) IR modes (see Figure S10). Figure 9 shows that pronounced narrowing of bands is also observed for the bands attributed to the N−H stretching modes, which appear in the region 3000−3300 cm^{-1}. Much more pronounced changes in fwhm for the modes related to NH_2 groups than $HCOO^-$ ions as well as very pronounced changes in the lattice mode region prove that ordering of FMD^+ cations plays a major role in the phase transition mechanism.

Broadening of Raman and IR bands upon heating of molecular crystals can be attributed mainly to phonon−phonon anharmonic interactions and increased reorientational motions of molecules or ions. When dynamic disorder prevails over the phonon decay process, the fwhm of a band can be expressed by

$$\text{fwhm} = A + BT + C\exp(-E_a/kT) \quad (3)$$

where E_a is the activation energy, k is the Boltzmann constant, and T is the temperature.[26] The first and second term correspond to the broadening due to structural or compositional defects and phonon−phonon anharmonic interactions, respectively. The third term of eq 3 describes the thermally activated reorientational processes. Figure 11 shows that the temperature dependence of the ρ(NH_2) IR-active mode can be well explained by eq 3 with the fitting parameters A = 5.5 cm^{-1}, B = 0.015 cm^{-1} K^{-1}, and E_a = 135 meV (13.03 kJ/mol). The value of E_a is larger than the 103 and 92 meV values found for the [NH_4][$Mg(HCOO)_3$] and [$(CH_3)_2NH_2$][$Mn(HCOO)_3$] compounds studied by us previously.[11,22] It is also worth mentioning that our analysis indicates that the contribution of the reorientational processes to the observed broadening becomes important above about 200 K, whereas below 200 K this contribution becomes negligible and the observed changes in fwhm are related to the anharmonicity. This behavior is different from that observed for [$(CH_3)_2NH_2$][$Mn(HCOO)_3$] and [NH_4][$Mg(HCOO)_3$], for which reorientational processes of NH_4^+ and DMA^+ cations contributed to the observed fwhm down to 100 K.[11,22]

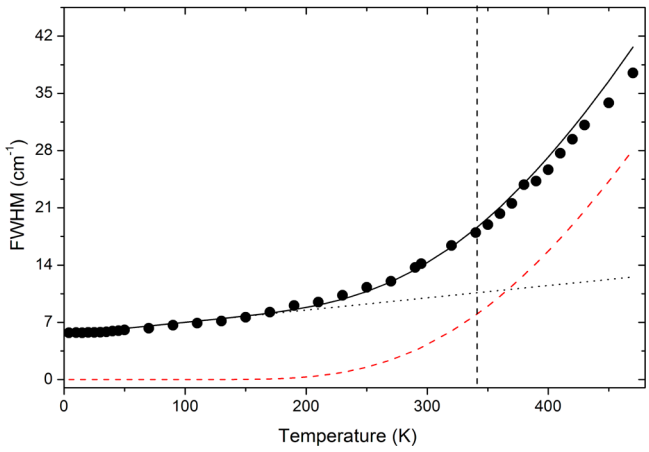

Figure 11. Temperature dependence of fwhm of the 1316 cm^{-1} IR band corresponding to the ρ(NH_2) mode. The black dotted line and red dashed line represent contributions due to anharmonicity and reorientational processes, respectively. The vertical line indicates the temperature at which FMDMn undergoes a phase transition.

DISCUSSION AND CONCLUSIONS

X-ray diffraction studies show that FMDMn belongs to the family of metal formate frameworks templated by organic cations, which present an ABO_3 perovskite architecture, in which the metal cations (B = M^{2+}) linked by formate groups (X = $HCOO^-$) form a BX_3 skeleton, and the A = organic cations occupy the cavities. It is, therefore, interesting to make a comparison with regard to ferroelectric properties and structural correlations. The high-temperature structure of FMDMn is similar to the room-temperature structure of [DMA][$Mn(HCOO)_3$]; that is, both structures have very similar metal formate frameworks containing large cavities occupied by disordered organic cations. In both cases the space group symmetry is $R\bar{3}c$. Figure 12 shows the comparison between these two structures. As can be noticed, in the DMAMn structure, the long axis of the DMA^+ ion is directed along the c axis, whereas in the FMDMn structure the planar FMD^+ cation is constrained to have the N−C−N bonds in the plane perpendicular to the c axis. Due to this difference, the lattice parameter c decreases from 22.886 Å for DMAMn to 19.5912 Å for FMDMn, whereas the lattice parameter a increases from 8.3315 Å for DMAMn to 8.8776 Å for FMDMn. In contrast to FMDMn, [FMD][$Zn(HCOO)_3$] and [FMD]-[$Mg(HCOO)_3$] crystallize in a different structure (space group *Pnna*) than [DMA][$Zn(HCOO)_3$] and [DMA][$Mg(HCOO)_3$] (space group $R\bar{3}c$).[13,27,28] This behavior can be attributed to the fact that the FMD^+ cation has a slightly larger ionic size than the DMA^+ cation.[29] Therefore, it still has enough place for disorder in FMDMn since due to the large size of the Mn^{2+} cations, the cavities formed in the manganese formate framework are large. However, for smaller Zn^{2+} and Mg^{2+} cations, the cavities are not large enough to allow rotation of the FDM^+ cations, and a different type of crystal structure is realized, with a more distorted metal formate framework of orthorhombic symmetry.

Our results show that the IR bands related to the N−H stretching modes are observed for FMDMn at about 100−150 cm^{-1} higher frequencies than the corresponding bands of DMAMn.[11] These results indicate that the FMD^+ cation forms weaker H-bonds with the formate units than the DMA^+ cation. Low-temperature X-ray diffraction data are consistent with this

dx.doi.org/10.1021/ic500479e | Inorg. Chem. 2014, 53, 5260−5268

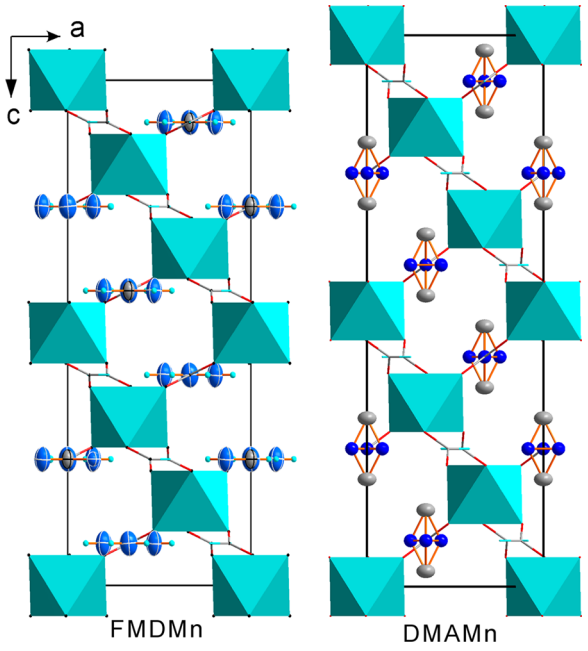

Figure 12. View of the crystal structure of FMDMn (T = 355 K) and DMAMn (T = 295 K) along the b direction in the rhombohedral phases. For FMDMn the displacement parameters for FMD^+ are drawn with 30% probability; for DMAMn hydrogen atoms are omitted for clarity.

conclusion, showing significantly longer N···O distances in the FMDMn structure (2.8570 and 2.8984 Å, see Table 2) than in the DMAMn structure (2.8313 and 2.8340 Å,[30]). In spite of the weaker individual H-bonds in FMDMn, the FMD^+ cations are more strongly bonded to the metal formate framework than the DMA^+ cations. Due to the presence of two NH_2 groups, they form four H-bonds to the anionic network, whereas the DMA^+ cations are able to form only two H-bonds. A tighter binding of the FMD^+ cation in the cavities correlates with significantly higher phase transition temperature into the disordered phase in FMDMn (about 336 K) than DMAMn (about 184 K[11]). It is also consistent with a large activation energy for the reorientational motion of the FMD^+ cation obtained from the analysis of the dielectric and vibrational data discussed above.

A comparison of magnetic properties of FMDMn and DMAMn shows that both compounds exhibit ferromagnetic order at very similar temperatures, i.e., 8.0 K for FMDMn and 8.5 K for DMAMn.[31] This result is consistent with very similar coordination spheres of the central Mn^{2+} ions, the *anti*–*anti* connection mode of the bridging formate, and similar distances between the Mn^{2+} ions in both compounds.

Different experimental methods used in the present study show that the phase transition in FMDMn has slightly first-order character, in contrast with a strongly first-order character in DMAMn. Temperature-dependent studies give also strong evidence that the phase transition in FMDMn has an order–disorder character and is governed by dynamics of the FMD^+ cations. Our results show that ordering of the FMD^+ cations is also associated with a significant distortion of the metal formate framework but very weak distortion of the FMD^+ cation itself. In particular, the FMD^+ cation remains nearly planar, with the two C–N bonds still equivalent in the low-temperature phase. Furthermore, the FMD^+ ions do not exhibit any significant tilting with respect to the anionic framework. This behavior is considerably different from that observed for DMAMn, for which substantial distortion below T_c was observed also for the DMA^+ cation. Here it is important to mention that theoretical considerations showed that in $[C(NH_2)_3][[Cu(HCOO)_3]$ the organic ion is the main source of polarization.[7,10] It was also suggested that using a different organic cation with more polarizable electron density would increase the polarization.[7,10] This conclusion is supported by theoretical studies of MOFs with a perovskite-like topology containing different organic ions such as $C(NH_2)_3^+$, $CH_3CH_2NH_3^+$, and $CF_3CH_2NH_3^+$.[8,9] These studies revealed that ferroelectric polarization in this class of compounds appears due to the peculiar canted ordering of the organic cation dipole moments. Thus, it is possible to tune the ferroelectric polarization by changing the magnitude and the canting of the organic molecular dipole.[9] Our results show that in spite of very similar structures of DMAMn and FMDMn compounds, and similar monoclinic distortion of the parent trigonal phase below T_c, the cooperative ordering of the FMD^+ cations leads to the centrosymmetric structure. Furthermore, in contrast to the MOFs containing $C(NH_2)_3^+$, $CH_3CH_2NH_3^+$, $CF_3CH_2NH_3^+$, etc., cations, the FMD^+ cations do not exhibit any significant tilting in the low-temperature phase. This very important difference in behavior of FMDMn and ferroelectric MOFs with a perovskite-like topology containing monoamino cations indicates that the size of the organic cation and its bonding strength to the anionic framework play a very important role in the stability of the structure and determine its properties. Very weak distortion and negligible tilt of the FMD^+ cation below T_c can be attributed to formation of extensive H-bonds between this diamino cation and the anionic framework.

In summary, we have synthesized a novel MOF with a perovskite-type topology containing FMD^+ cations in the cavities of the framework and analyzed the mechanism of the structural phase transition observed in this compound above room temperature. Our analysis has deepened the understanding of the structure–property relationship of this class of MOFs.

■ ASSOCIATED CONTENT

Supporting Information

X-ray crystallographic information files (CIF) for crystal structures of FMDMn at 355, 295, and 110 K. Figures S1–S10: powder X-ray diffraction, DSC traces, the content of the asymmetric unit, view of the crystal structures, IR and Raman spectra, temperature dependence of bandwidths and frequencies. Tables S1–S4: X-ray data collection and refinement parameters, selected bond angles, the correlation diagram showing the correspondence between the optical modes in the $R\bar{3}c$ and $C2/c$ structures, and Raman and IR frequencies for DMFMn together with the proposed assignment. This material is available free of charge via the Internet at http://pubs.acs.org.

■ AUTHOR INFORMATION

Corresponding Author

*E-mail: m.maczka@int.pan.wroc.pl. Phone: +48-713954161. Fax: +48-713441029.

Author Contributions

The manuscript was written through contributions of all authors. All authors have given approval to the final version of the manuscript.

Notes

The authors declare no competing financial interest.

■ ACKNOWLEDGMENTS

This research was supported by the National Center for Science (NCN) in Poland under project No. DEC-2011/03/B/ST5/01019.

■ REFERENCES

(1) Kreno, L. E.; Leong, K.; Farha, O. K.; Allendorf, M.; Van Duyene, R. P.; Hupp, J. T. *Chem. Rev.* **2012**, *112*, 1105−1125.
(2) Zhang, W.; Xiong, R. G. *Chem. Rev.* **2012**, *112*, 1163−1195.
(3) (a) Rogez, G.; Viart, N.; Drillon, M. *Angew. Chem., Int. Ed.* **2010**, *49*, 1921−1923. (b) Ramesh, R. *Nature* **2009**, *461*, 1218−1219.
(4) (a) Jain, P.; Ramachandran, V.; Clark, R. J.; Zhou, H. D.; Toby, B. H.; Dalal, N. S.; Kroto, H. W.; Cheetham, A. K. *J. Am. Chem. Soc.* **2009**, *131*, 13625−1327. (b) Guo, M.; Cai, H. L.; Xiong, R. G. *Inorg. Chem. Commun.* **2010**, *13*, 1590−1598. (c) Fu, D. W.; Zhang, W.; Cai, H. L.; Zhang, Y.; Ge, J. Z.; Xiong, R. G.; Huang, S. D.; Nakamura, T. *Angew. Chem., Int. Ed.* **2011**, *50*, 11947−11951.
(5) Xu, G. C.; Zhang, W.; Ma, X. M.; Hen, Y. H.; Zhang, L.; Cai, H. L.; Wang, Z. M.; Xiong, R. G.; Gao, S. *J. Am. Chem. Soc.* **2011**, *133*, 14948−14951.
(6) Wang, W.; Yan, L.-Q.; Cong, J.-Z.; Zhao, Y.-L.; Wang, F.; Shen, S.-P.; Zhou, T.; Zhang, D.; Wang, S.-G.; Han, X.-F.; Sun, Y. *Sci. Rep.* **2013**, *3*, 2024.
(7) Stroppa, A. *J. Phys. Conf. Ser.* **2013**, *428*, 012029.
(8) Stroppa, A.; Barone, P.; Jain, P.; Perez-Mato, J. M.; Picozzi, S. *Adv. Mater.* **2013**, *25*, 2284−2290.
(9) Di Sante, D.; Stroppa, A.; Jain, P.; Picozzi, S. *J. Am. Chem. Soc.* **2013**, *135*, 18126−18130.
(10) Stroppa, A.; Jain, P.; Barone, P.; Marsman, M.; Perez Mato, J. M.; Cheetham, A. K.; Kroto, H. W.; Picozzi, S. *Angew. Chem., Int. Ed.* **2011**, *50*, 5847−5850.
(11) Mączka, M.; Gągor, A.; Macalik, B.; Pikul, A.; Ptak, M.; Hanuza, J. *Inorg. Chem.* **2014**, *53*, 457−467.
(12) (a) Rossin, A.; Giambiastiani, G.; Peruzzini, M.; Sessoli, R. *Inorg. Chem.* **2012**, *51*, 6962−6968. (b) Ma, X.; Tian, J.; Yang, H. Y.; Zhao, K.; Li, X. *J. Solid State Chem.* **2013**, *201*, 172−177.
(13) (a) Marsh, R. E. *Acta Crystallogr. C* **1986**, *42*, 1327−1328. (b) Rossin, A.; Chierotti, M. R.; Giambiastiani, G.; Gobetto, R.; Peruzzini, M. *CrystEngComm* **2012**, *14*, 4454−4460.
(14) Stoumpos, C. C.; Malliakas, C. D.; Kanadzidis, M. G. *Inorg. Chem.* **2013**, *52*, 9019−9038.
(15) *CrysAlisCCD* and *CrysAlis RED*, version 1.171.33.42; Oxford Diffraction Ltd., 2009.
(16) Sheldrick, G. M. *Acta Crystallogr. A* **2008**, *64*, 112−122.
(17) (a) Samantaray, R.; Clark, R. J.; Choi, E. S.; Zhou, H.; Dalal, N. S. *J. Am. Chem. Soc.* **2011**, *133*, 3792−3795. (b) Samantaray, R.; Clark, R. J.; Choi, E. S.; Dalal, N. S. *J. Am. Chem. Soc.* **2012**, *134*, 15953−15962.
(18) Tetsuo, A.; Ashitomi, K. *J. Phys. Chem. C* **2013**, *117*, 10185−10190.
(19) Besara, T.; Jain, P.; Dalal, N. S.; Kuhns, P. L.; Reyes, A. P.; Kroto, H. W.; Cheetham, A. K. J. *Proc. Natl. Acad. Soc.* **2011**, *108*, 6828−6832.
(20) (a) Kageyama, H.; Khomskii, D. I.; Levitin, R. Z.; Markina, M. M.; Okuyama, T.; Uchimoto, T.; Vasil'ev, A. N. *J. Magn. Magn. Mater.* **2003**, *262*, 445−451. (b) Mao, J.; Sui, Y.; Zhang, X.; Su, Y.; Wang, X.; Liu, Z.; Wang, Y.; Zhu, R.; Wang, Y.; Liu, W.; Tang, J. *Appl. Phys. Lett.* **2011**, *98*, 192510. (c) Dasari, N.; Mandal, P.; Sundaresan, A.; Vidhyadhiraja, N. S. *Europhys. Lett.* **2012**, *99*, 17008.
(21) (a) Dzyaloshinsky, I. *J. Phys. Chem. Solids* **1958**, *4*, 241−255. (b) Moriya, T. *Phys. Rev.* **1960**, *120*, 91−98.
(22) (a) Maczka, M.; Pietraszko, A.; Macalik, B.; Hermanowicz, K. *Inorg. Chem.* **2014**, *53*, 787−794. (b) Zhang, R.; Xu, G. C.; Wang, Z. M.; Gao, S. *Chem.—Eur. J.* **2013**, *20*, 1146−1158.
(23) (a) Maczka, M.; Hanuza, J.; Kaminskii, A. A. *J. Raman Spectrosc.* **2006**, *37*, 1257−1264. (b) Magalhaes, A. L.; Madail, S. R. R. S.; Ramos, M. *J. Theor. Chem. Acc.* **2000**, *105*, 68−76.
(24) (a) Bator, G.; Zeeger-Huyskens, T.; Jakubas, R.; Zaleski, J. *J. Mol. Struct.* **2001**, *570*, 61−74. (b) Magalhaes, A. L.; Gomes, J. A. N. F. *Int. J. Quantum Chem.* **1997**, *61*, 725−739. (c) Drozd, M.; Dudzic, D. *Spectrochim. Acta, Part A* **2013**, *115*, 345−356.
(25) (a) Durig, J. R.; Bush, S. F.; Baglin, F. G. *J. Chem. Phys.* **1968**, *49*, 2106−2117. (b) Sobczyk, L.; Obrzyd, M.; Filarowski, A. *Molecules* **2013**, *18*, 4467−4476.
(26) Carabatos-Nedelec, C.; Becker, P. *J. Raman Spectrosc.* **1997**, *28*, 663−671.
(27) Jain, P.; Dalal, N. S.; Toby, B. H.; Kroto, H. W.; Cheetham, A. K. *J. Am. Chem. Soc.* **2008**, *130*, 10450−10451.
(28) Pato-Doldan, B.; Sanchez-Andujar, M.; Gomez-Aguirre, L. C.; Yanez-Vilar, S.; Lopez-Beceiro, J.; Gracia-Fernandez, C.; Haghighirad, A. A.; Ritter, F.; Castro-Garcia, S.; Senaris-Rodrigues, M. A. *Phys. Chem. Chem. Phys.* **2012**, *14*, 8498−8501.
(29) (a) Mitzi, D. B.; Liang, K. *J. Solid State Chem.* **1997**, *134*, 376−381. (b) Knutson, J. L.; Martin, J. D.; Mitzi, D. B. *Inorg. Chem.* **2005**, *44*, 4699−4705.
(30) Sanchez-Andujar, M.; Presedo, S.; Yanez-Vilar, S.; Castro-Garcia, S.; Shamir, J.; Senaris-Rodrigues, M. A. *Inorg. Chem.* **2010**, *49*, 1510−1516.
(31) Wang, X. Y.; Gan, L.; Zhang, S. W.; Gao, S. *Inorg. Chem.* **2004**, *43*, 4615−4625.